

Article

# Design and Research on DC Electric Leakage Protection Circuit Breaker

Lei Hou <sup>1</sup>, Dezhi Chen <sup>2,\*</sup>, Tongfei Li <sup>2</sup>, Ming Zhao <sup>3</sup> and Huaibo Ren <sup>1</sup>

<sup>1</sup> State Grid Hebei Electric Power Co., Ltd., Xiongan New Area Power Supply Company, Baoding 071000, China; zp13546284672@163.com (L.H.); lxz6958@163.com (H.R.)

<sup>2</sup> School of Electrical Engineering, Shenyang University of Technology, Shenyang 110870, China; 18713908532@163.com

<sup>3</sup> State Grid Hebei Electric Power Co., Ltd., Shijiazhuang 050022, China; zhengyang19980605@163.com

\* Correspondence: chendezhi@sut.edu.cn; Tel.: +86-187-1390-8532

**Abstract:** In recent years, DC power supply and distribution technology plays an increasingly significant role in power supply and distribution systems with a low loss and large power supply radius. However, the corresponding DC distribution network protection electric devices cannot satisfy the needs of the existing DC power supply and distribution network. Based on this, in this article, an intelligent/energy-efficient DC leakage protection circuit breaker based on two-phase magnetic nanomaterials and detection and control technology is proposed. Firstly, the core of an intelligent/energy-efficient DCCB is composed of two-phase magnetic nanomaterials, and the mathematical modeling process, preparation and processing method of two-phase magnetic nanomaterials are given. Secondly, the DC leakage detection technology is studied by fluxgate technology, and the design process of magnetic rings, winding and detection circuit is given. Thirdly, the simulation and experiment results of the detection system and actuator are given by the simulation and experiment of an intelligent/energy-efficient DCCB to verify the correctness of the proposed scheme.

**Keywords:** DC distribution network; two-phase magnetic nanomaterials; leakage circuit breaker; intelligent/energy-efficient; simulation and experiment



**Citation:** Hou, L.; Chen, D.; Li, T.; Zhao, M.; Ren, H. Design and Research on DC Electric Leakage Protection Circuit Breaker. *Energies* **2022**, *15*, 5605. <https://doi.org/10.3390/en15155605>

Academic Editors: Gian Giuseppe Soma and Mario Marchesoni

Received: 16 December 2021

Accepted: 30 March 2022

Published: 2 August 2022

**Publisher's Note:** MDPI stays neutral with regard to jurisdictional claims in published maps and institutional affiliations.



**Copyright:** © 2022 by the authors. Licensee MDPI, Basel, Switzerland. This article is an open access article distributed under the terms and conditions of the Creative Commons Attribution (CC BY) license (<https://creativecommons.org/licenses/by/4.0/>).

## 1. Introduction

In recent years, with the extensive access to distributed renewable energy, energy storage systems and DC load in power grids, DC power distribution systems and DC power supply systems have received extensive attention [1]. A lot of work has been done on the topology, simulation model, control strategy and system analysis in the process of AC to DC conversion [2–4]. However, there is a lack of research on the protection equipment of DC distribution systems and power supply systems, such as DC air circuit breaker, DC leakage protector, DC connector, etc.

A circuit breaker is an automatic control appliance used to frequently connect or disconnect electrical circuits [5]. It is widely used in automatic control systems and has the advantages of a large control capacity and remote operation [6,7]. The traditional AC circuit breaker cannot detect the DC current, so it cannot be protected. Even when there is a high-frequency leakage current or DC leakage current component, it will lose the basic AC leakage protection function [8–10]. The B-type sensor that can detect DC leakage has a high price, large volume and cannot grasp the production and supply situation [11,12]. Therefore, the development of a circuit breaker with a leakage protection function is of great significance [13]. On the other hand, during recent decades, DCCBs have been deeply investigated in industry and academia. There has been impressive progress in terms of efficiency, response time, power-density, lifetime and electrical operating ratings [14]. However, the traditional circuit breaker still has some shortcomings, such as high energy consumption, high calorific value, short service life, narrow application range of working

voltage, low voltage working difference and high and low voltage cannot be taken into account [15].

Based on this, this paper innovatively composed the stator core of a new DC leakage protector (intelligent/energy-saving DC leakage protection circuit breaker) by nano two-phase magnetic material and carried out DC magnetization and demagnetization of the stator core. The remanence was used to make the contactor close, which can effectively reduce energy consumption. At the same time, a single-core single-winding structure is used as excitation winding and measurement winding, and the fluxgate current sensing chip is designed. It can effectively detect the DC leakage current and form a new DC leakage protector with a DC leakage protection function. Finally, a prototype is manufactured, and the simulation and experiment are carried out to verify the correctness of the proposed scheme.

## 2. System Overview

Figure 1 shows the main structure of the new DC leakage protector. As shown in Figure 1, the new DC leakage protector mainly includes detection and control system, main contact, moving core, static core and reset spring, etc.

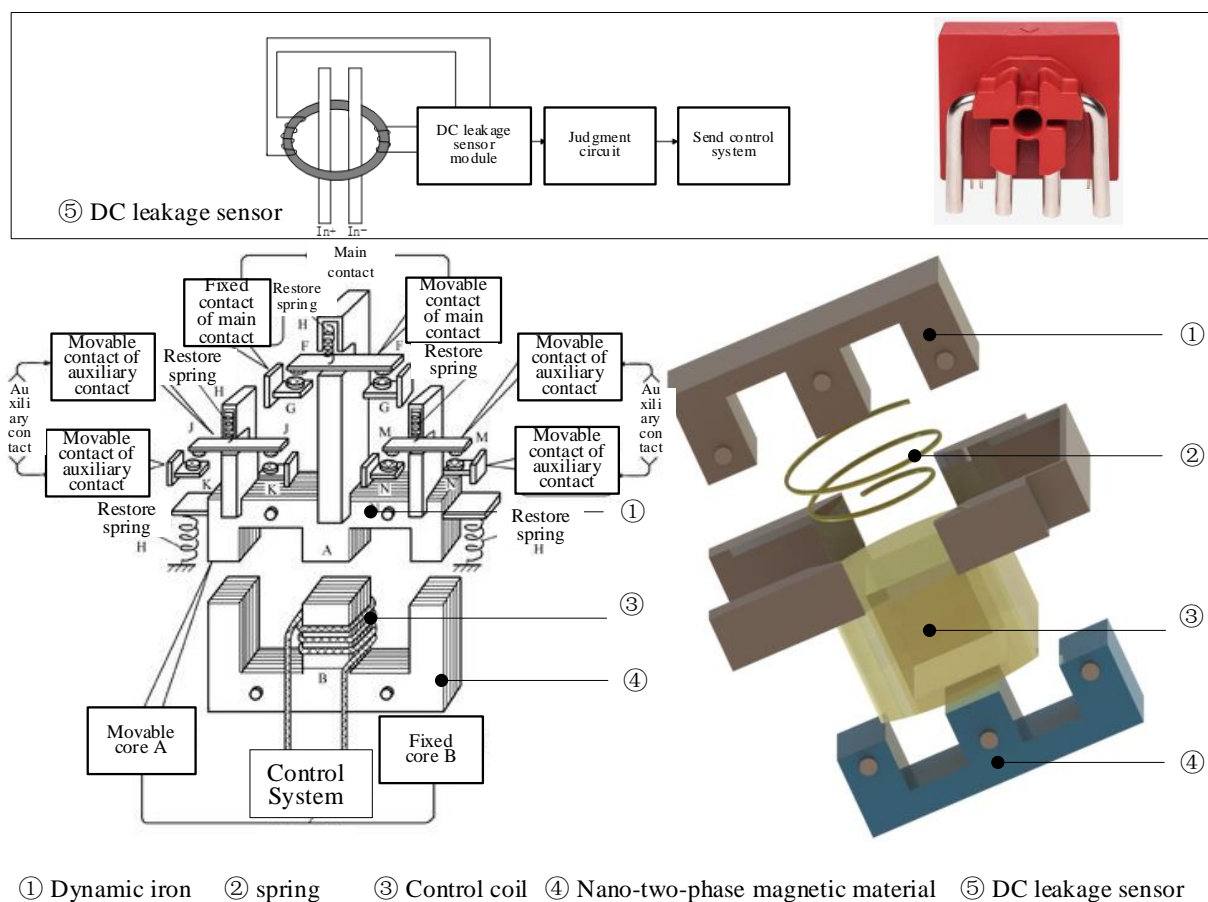


**Figure 1.** Main structure of the new DC leakage protector.

According to the structure of the new DC leakage protector shown in Figure 1, when the control winding flows into the DC 20 min, the two-phase magnetic material is excited, the two-phase magnetic material is characterized by permanent magnet properties, and the DC leakage protector starts working. When the DC leakage sensor detects a leakage failure, the control winding rapidly accesses AC power, makes two-phase magnetic materials, and the DC leakage protector cut circuit to complete protection.

### 3. Characteristic Modeling and Preparation of Nano Two-Phase Magnetic Materials

In this paper, a macro hysteresis model of nano-two-phase magnetic materials is established based on the Preisach model theory. The hysteresis characteristics of nano-two-phase magnetic materials are calculated to provide theoretical basis for circuit breaker prototype. The basic principle of the Preisach hysteresis model is to express the hysteresis characteristics of magnetic material as a set of magnetic dipoles with rectangular hysteresis characteristics. When ferromagnetic material is not magnetized, the number of forward and reverse magnetic dipoles with rectangular hysteresis characteristics is the same, and the material is not magnetic [16–18]. The Preisach diagram under different states is shown in Figure 2.

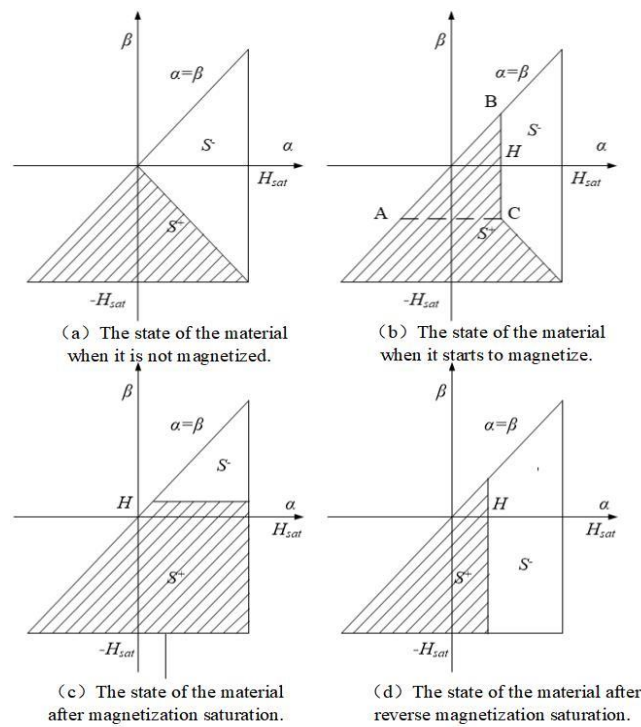


Figure 2. Preisach diagram under different states.

Corresponding to Figure 2a:

$$B = \iint_{S^+} \mu(\alpha, \beta) d\alpha d\beta - \iint_{S^-} \mu(\alpha, \beta) d\alpha d\beta = 0, \tag{1}$$

When the material begins to magnetize, the corresponding Preisach diagram is shown in Figure 2b, and the corresponding magnetic induction intensity can be expressed as:

$$B_i = \iint_{S^+} \mu(\alpha, \beta) d\alpha d\beta - \iint_{S^-} \mu(\alpha, \beta) d\alpha d\beta = T(H, -H) \tag{2}$$

with

$$T(\alpha, \beta) = \int_{\beta}^{\alpha} \int_y^{\alpha} \mu(\alpha, \beta) dx dy = \int_{\beta}^{\alpha} \int_{\beta}^x \mu(\alpha, \beta) dx dy \tag{3}$$

In the formula, the area integral  $T(\alpha, \beta)$  of the triangle has  $(\alpha, \beta)$  as its vertex. In Figure 2b,  $T(H, -H)$  can be equivalent to the area of triangle ABC. It can be concluded from the above that  $T(\alpha, \beta) = T(-\alpha, -\beta)$ , and  $B_i$  is the magnetic induction intensity of the initial magnetization curve.

After the magnetic material is magnetized to saturation, with the decrease of the magnetic field intensity, the magnetic induction intensity changes in the descent trajectory of the limit hysteresis loop. The Preisach diagram of this process is shown in Figure 2c, which can be expressed as:

$$\begin{aligned} B_d &= \iint_{S^+} \mu(\alpha, \beta) d\alpha d\beta - \iint_{S^-} \mu(\alpha, \beta) d\alpha d\beta \\ &= B_i(H_{sat}) - 2T(H_{sat}, H) \end{aligned} \quad (4)$$

In the formula,  $B_d$  represents the magnetic induction intensity on the descending branch.

$$\begin{aligned} B_u &= \iint_{S^+} \mu(\alpha, \beta) d\alpha d\beta - \iint_{S^-} \mu(\alpha, \beta) d\alpha d\beta \\ &= -B_i(H_{sat}) + 2T(H, -H_{sat}) \end{aligned} \quad (5)$$

When the magnetization process includes local hysteresis loops, assuming that there are  $n$  local extreme points on the magnetization curve, the magnetic flux density on the descent trajectory can be expressed as:

$$B(H) = B(H_n) - 2T(H_n, H), \quad (6)$$

The magnetic density of the rising branch can be expressed as:

$$B(H) = B(H_n) + 2T(H, H_n), \quad (7)$$

In the above formula,  $H_n$  is the magnetic field intensity of the  $n$ th extreme point,  $B(H_n)$  is the magnetic induction intensity of the  $n$ th extreme point, and  $T(\alpha, \beta)$  can be expressed as:

$$T(\alpha, \beta) = \frac{B_u(\alpha) - B_d(\beta)}{2} + F(\alpha)F(\beta) \quad (8)$$

In the formula,  $B_d$  and  $B_u$  are the magnetization trajectories on the falling and rising branches of the limit hysteresis loop, respectively.

$$F(\alpha) = \frac{B_d(\alpha) - B_u(\alpha)}{2\sqrt{B_d(\alpha)}} (\alpha \geq 0) \quad (9)$$

$$F(\alpha) = \sqrt{B_d(-\alpha)} (\alpha \leq 0) \quad (10)$$

According to Formulas (9) and (10) calculate  $F(\alpha)$ , and then calculate  $T(\alpha, \beta)$ , only the magnetic induction intensity data of the ultimate hysteresis loop is used, without considering the distribution function  $\mu(\alpha, \beta)$ . Figure 3 shows the hysteresis loop of nano two-phase magnetic materials based on the Preisach model.

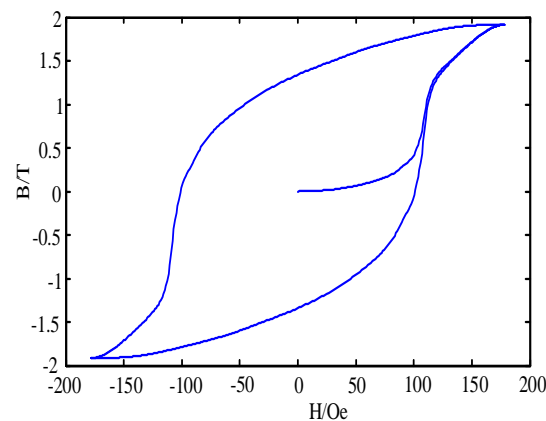
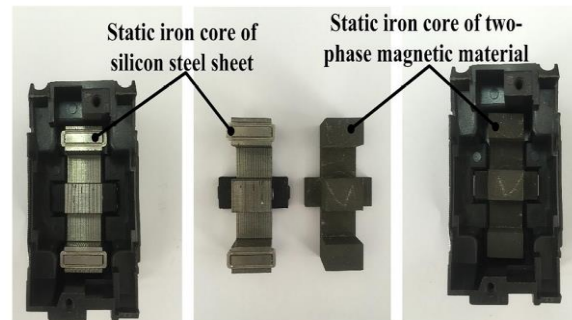


Figure 3. Hysteresis loop of two-phase magnetic material.

The hysteresis retaining of the two-phase magnetic material shown in Figure 3 can determine the relationship between the coercive force and the residual magnetic, and the nano-phase magnetic material can be prepared. Among them, the heat treatment process of nano-two-phase magnetic materials is as follows: two-phase magnetic materials are heat treated with a 5-stage tempering process. The specific implementation is as follows:  $620\text{ }^{\circ}\text{C} \times 1\text{ h} + 610\text{ }^{\circ}\text{C} \times 1\text{ h} + 590\text{ }^{\circ}\text{C} \times 2\text{ h} + 570\text{ }^{\circ}\text{C} \times 3\text{ h} + 560\text{ }^{\circ}\text{C} \times 3\text{ h}$ . Figure 4 shows the iron core of the nano-two-phase magnetic material prepared.



**Figure 4.** The core of circuit breaker with leakage protection of nano-two-phase magnetic material.

As shown in Figure 4, the leakage protector electromagnetic actuator mainly includes two portions of the dynamic core (silicon steel sheet material) and the static iron core (two-phase magnetic material), winding the windings in the static iron, to achieve the opening of the leakage protector and turn off.

#### 4. Design of DC Leakage Sensor

##### 4.1. Leakage Current Detection of Single-Winding Single-Core Fluxgate

The detection method of fluxgate detection technology is to superimpose the modulated excitation source of the magnetic ring in advance. Once there is current flowing in the magnetic ring, the waveform of the excitation source will change. The current is detected by demodulating the waveform of the excitation source. This detection method is characterized by strong small current measurement ability and is not easy to be disturbed, and it is very effective for the mA level leakage current detection [19].

Based on the fluxgate detection principle, a single-core and single-winding detection method is proposed in this paper. The detection winding and excitation winding are integrated into one winding. The magnetic core works in the deep saturation region under the excitation of square wave voltage. The differential leakage current in the positive and negative buses is obtained by detecting the current change in the winding. Figure 5 shows the schematic diagram and equivalent circuit of fluxgate DC leakage current sensor.

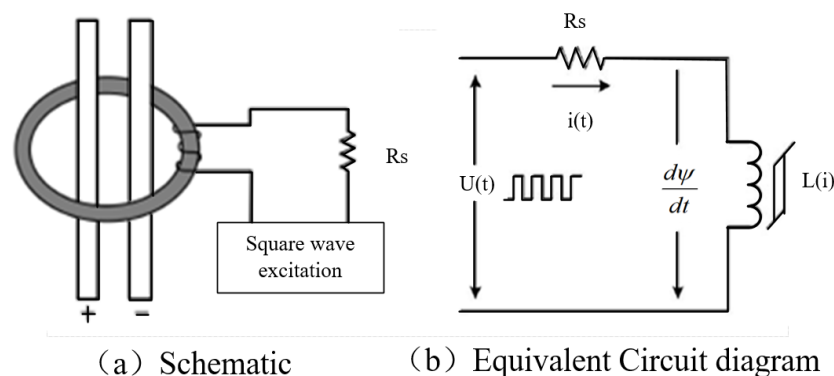


**Figure 5.** Schematic diagram and equivalent circuit of fluxgate DC leakage current sensor fluxgate DC leakage current sensor.

As shown in Figure 5, the excitation voltage  $U(t)$  is an ideal square wave, then the circuit equation of the circuit is

$$U(t) = i(t) \cdot R + \frac{d\psi}{dt} \quad (11)$$

In the formula,  $\psi$  is the total flux linkage linked by the excitation winding. According to Ampere's loop theorem:

$$H(t) \cdot l = N_2 \cdot i(t) \quad (12)$$

where  $l$  is the average magnetic circuit length of the toroidal core,  $N_2$  is the number of turns of the excitation winding, and  $i(t)$  is the instantaneous current in the loop.

$$\psi(t) = N_2\phi(t) = N_2B(t)S \quad (13)$$

$$B(t) = \mu(i)\mu_0H(t) \quad (14)$$

So

$$U(t) = i(t) \cdot R + \mu(i)\mu_0 \cdot N_2^2 \cdot \frac{S}{l} \cdot \frac{di(t)}{dt} \quad (15)$$

Among them,  $\mu(i)$  is the dynamic relative permeability of the magnetic core;  $\mu_0$  is the vacuum magnetic permeability  $4\pi \times 10^{-7}$  Wb/(A·m);  $S$  is the cross-sectional area of the magnetic core.

When the leakage current in the positive and negative buses is zero, assuming that the negative voltage just ends at time  $t_0$  and the magnetic core is in negative saturation, the circuit equation is written in sections as follows:

$$\begin{cases} U_{pp} = i(t)R + L_1 \frac{di(t)}{dt}, 0 < t < t_1 \\ U_{pF} = i(t)R + L_2 \frac{di(t)}{dt}, t_1 < t < t_2 \\ U_{pp} = i(t)R + L_3 \frac{di(t)}{dt}, t_2 < t < t_\infty \\ L_j = \mu_0\mu_j \cdot \frac{N_2^2 S}{l}, j = 1, 2, 3 \end{cases} \quad (16)$$

In the formula, the  $U_{pp}$  is the peak value of the added subsided voltage, and  $L_1$  is the self-induction of the magnetic core in the positive and negative saturation segment and the linear segment, and  $t_1$  is the start time of the linear segment,  $t_2$  is the hour, resulting.

$$\begin{cases} i = I_\infty \left(1 - 2e^{-\frac{t}{\tau_1}}\right), 0 < t < t_1 \\ i = I_n + (-I_s - I_n)e^{-\frac{t-t_1}{\tau_2}}, t_1 < t < t_2 \\ i = I_\infty + (I_s - I_{0s})e^{-\frac{t-t_2}{\tau_1}}, t_2 < t < t_{n0} \\ t_1 = \tau_1 \ln\left(\frac{2I_\infty}{I_n + I_s}\right) \\ t_2 = \tau_2 \ln\left(\frac{I_\infty + I_s}{I_\infty - I_s}\right) + t_1 \end{cases} \quad (17)$$

In the formula,  $\tau_1 = \frac{L_1}{R_s}$ ,  $\tau_2 = \frac{L_2}{R_f}$ ;  $I_s$  is the current in the sensor windings in the magnetic saturation,  $I_* = \frac{H_1 l}{N_2}$  and  $I_\infty$  is the maximum value of the current in the winding,  $I_\infty = \frac{U_m}{2R_n}$ .

As shown in Figure 6, since the magnetic core operating current is symmetrical, the current waveform of the latter half cycle can be obtained from the current waveform of the first half cycle. In view of  $L_2 \gg L_1 = L_3$  and  $L_1 = L_3 \approx 0$ ,  $L_3 \gg T_\infty/2$  (the transition process is sufficiently short), the magnetic core current waveform can be further approximately as

shown in Figure 6, the cycle of the current waveform depends mainly on the rise time and fall time of the linear segment, which is:

$$\begin{aligned}
 T &\approx 2\tau_2 \ln\left(\frac{I_m + I_s}{I_0 - I_s}\right) \\
 &= 2\frac{\mu_0\mu_2 N_2^2 S}{R_s l} \ln\left(1 + \frac{2}{\frac{N_2 U_{pp}}{2R_s H_s l} - 1}\right)
 \end{aligned}
 \tag{18}$$

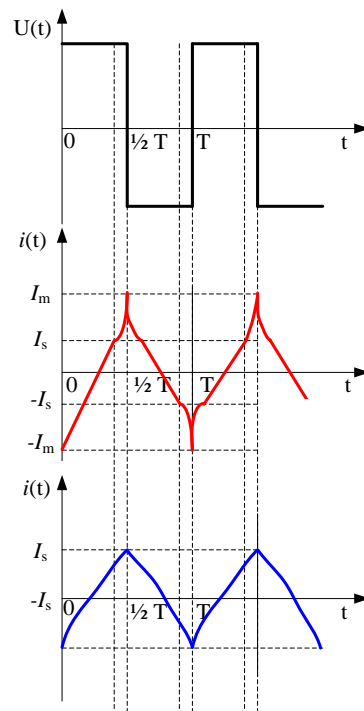


Figure 6. Excitation voltage and current waveform in winding.

When there is a forward leakage current  $I_0$  in the positive and negative bus, the magnetic field intensity in the magnetic core is:

$$H = \frac{N_1 I_0}{l} + \frac{N_2 i(t)}{l}
 \tag{19}$$

Among them,  $N_1$  is the number of turns on one side,  $N_1 = 1$ ;

$$H = \frac{I_0}{l} + \frac{N_2 i(t)}{l} = \frac{N_2 \left[ i(t) + \frac{I_0}{N_2} \right]}{l} = \frac{N_2 i(t)}{l}
 \tag{20}$$

Since the current  $i(t)$  in the excitation winding is obtained on the sampling resistance, it can be seen from Equation (15) that the role of  $I_0$  is actually equivalent to pulling the  $i(t)$  vertical direction  $I_0/N_2$ , as shown in Figure 7a; similarly, when there is a negative DC leakage current  $-I_0$ , it is equivalent to translating  $i(t)$  upward along the longitudinal axis  $I_0/N_2$ , as shown in Figure 7b.

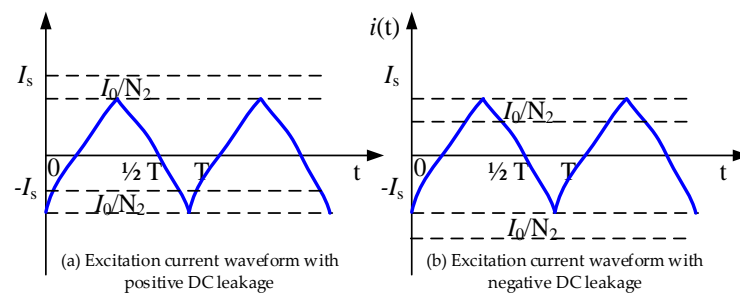


**Figure 7.** Excitation current waveform with DC leakage.

Since the monomagnetic current is a nonlinear cycle signal, the DC leakage current is to be detected, and the characteristics of the signal need to be analyzed, and it is found that the feature amounts that can represent the leakage signal can be found. Since the Fourier exhibition of the applied square wave exciting voltage is:

$$U(t) = \frac{2U_m}{\pi} \left( \cos \omega_1 t - \frac{1}{3} \cos 3\omega_1 t + \frac{1}{5} \cos 5\omega_1 t - \dots \right) \quad (21)$$

When there is a DC leakage current  $I_0$  in the busbar, it can be obtained according to the superposition theorem of the circuit.

$$i(t) = \frac{2U_{N2}}{\pi} \left( \frac{1}{R_x + j\omega_1 L_2} \cos \omega_1 t - \frac{1}{3} \cdot \frac{\cos 3\omega_1 t}{R_x + j3\omega_1 L_2} + \frac{1}{5} \cdot \frac{\cos 5\omega_1 t}{R_2 + j5\omega_2 L_2} - \dots \right) + \frac{I_0}{N_2} \quad (22)$$

As can be seen from the Formula (17), only the DC component and the wholly harmonic component are contained in  $i(t)$  and the DC component is proportional to the DC leakage current  $I_0$ , so high frequency components can be used by design appropriate low pass filters. Filter is filtered to obtain a direct current leakage signal, and adaptive detection is achieved according to this.

The common values of the operating current of the DC leakage protector are 10 mA, 30 mA, 100 mA, and 300 mA; 30 mA is the maximum value for human protection, and 300 mA is the maximum value for fire protection. IEC60479-1 shows that when the current flows through one hand and one foot of the human body and the current is greater than 30 mA, it may cause death. Unless the current is cut off quickly, the operating current of the leakage protector for human protection shall not exceed 30 mA. This DC leakage current sensing module can detect a leakage current of 30 mA, which meets the needs of personal safety protection; this DC leakage current sensing module can detect a leakage current of 300 mA, which meets the requirements of fire safety protection. The DC leakage protector can be very suitable for personal and fire protection scenarios and has a good market prospect.

According to the characteristics of single-winding and single-core fluxgate detection technology, the magnetic core with high permeability, low coercivity and good rectangular hysteresis loop characteristics is needed. Based on this, permalloy material is used as the magnetic core material in this paper. Figure 8 shows the core hysteresis loop.

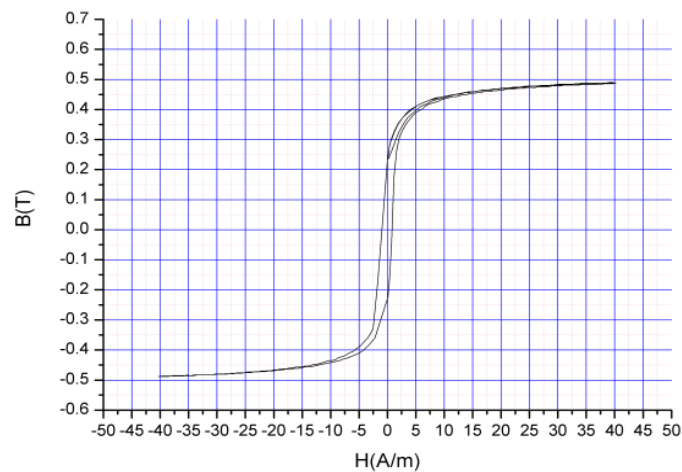


**Figure 8.** Hysteresis loop of magnetic core.

#### 4.2. Chip Design

Based on the study of fluxgate analog circuit, the core sensing excitation detection circuit was designed, and auxiliary modules were added. The overall chip layout was designed, and the layout of each module of the analog RF front-end was designed to carry out the layout and wiring of the circuit and complete the final layout integration. Figure 9 shows the functional block diagram of fluxgate current sensor chip. Figure 10 shows the Soc chip integration design. After designing Soc, the chip was manufactured. The chip size was  $1.72 \text{ mm} \times 1.72 \text{ mm}$ , the PAD window size was  $0.09 \text{ mm} \times 0.09 \text{ mm}$ , and the power supply was DC5 V. Figure 11 shows the Soc chip designed in this paper.

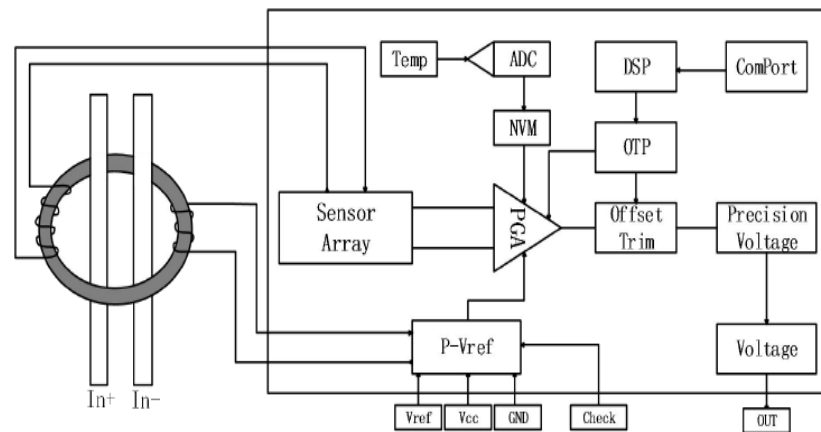


**Figure 9.** Magnetic flux gate current sensing chip function block diagram.

As shown in Figure 12, the module in this paper adopts a single magnetic core and a single winding structure. The detection winding and the excitation winding are combined into one. The magnetic core works in a deep saturation state under the excitation of a square wave voltage. By detecting the current change in the winding, the differential leakage current of the positive and negative busbars can be obtained, which simplifies the structure of the sensor and makes the volume of the sensor very small, which can be applied to many scenarios with high space requirements, and also improves the working reliability.

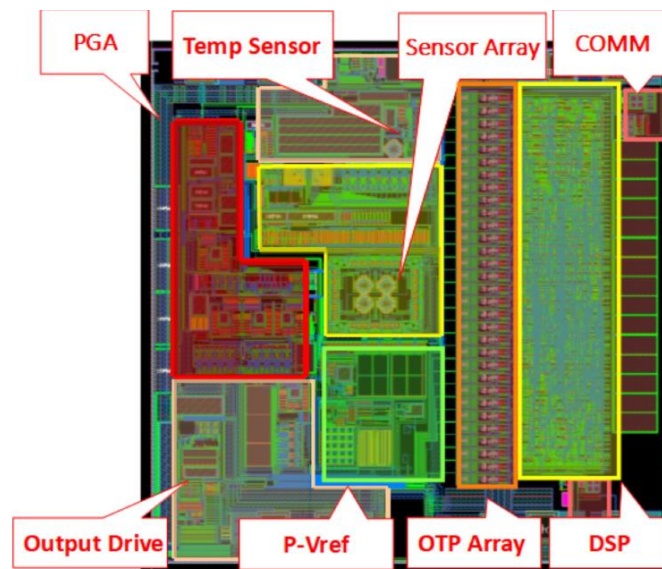


Figure 10. Integrated design diagram of SOC chip.

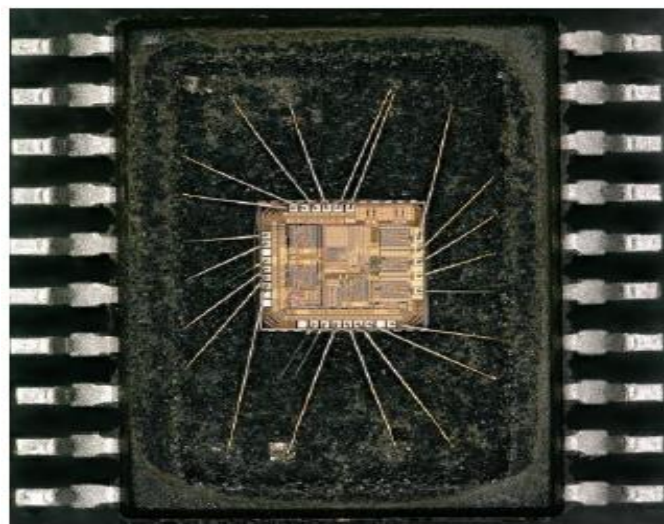


Figure 11. Perspective of the chip.

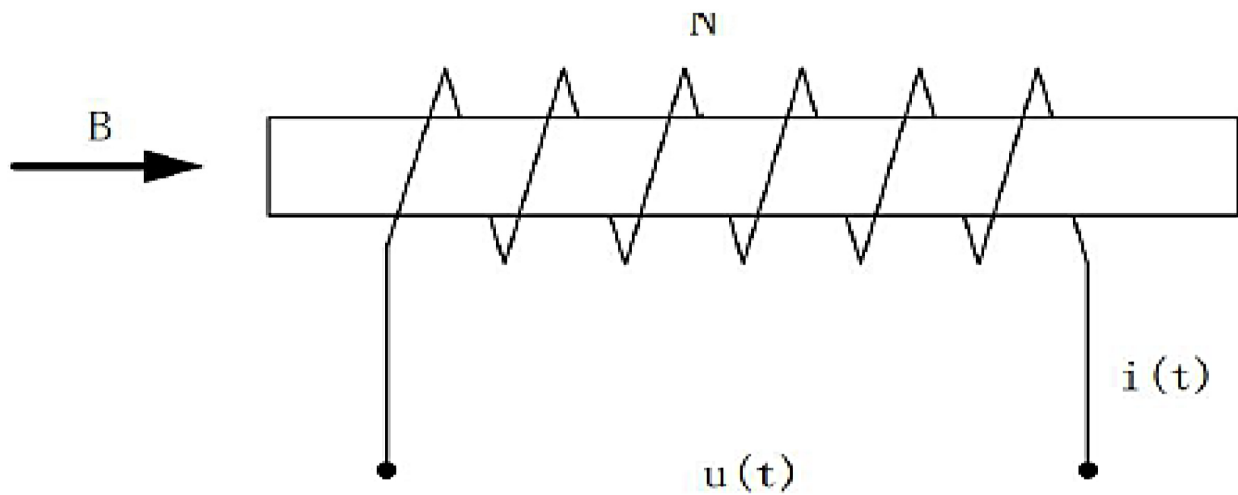


Figure 12. The structure of single-core winding fluxgate structure.

For proportional amplification of coupled leakage current signals, low-pass KRC-Sallen–Key filter is adopted. Its gain unit consists of a noninverting amplifier and two RC filters combined in combination with operational amplifier to form a second-order active low-pass filter, and a two-stage structure is used to form a fourth-order active low-pass filter.

As shown in Figure 10, each part of the function is briefly described as follows:

- (1) PGA: The programmable gain adjustment module, is used to adjust the sensor gain without manually adjusting the resistance, which can be modified by programming.
- (2) Temp sensor: Temperature compensation module, temperature calibration, used to compensate for the phenomenon of the leakage current.
- (3) Sensor Array: Sensing excitation detection arrays, generating excitation, while detecting signals after the magnetic core coupled.
- (4) COMM: Communication interface, read data onto external communication, and the program burning.
- (5) Output Drive: Output drivers, output drivers, increase the output current of the module, so that the sensor output is more stable.
- (6) P-Vref: Adjustable reference voltage output, programmable reference, adjustment reference voltage value (sensor V-ref is automatically adjusted, can be 2.5 V or 1.25 V, etc.).
- (7) OTP: Disposable programmable module.
- (8) DSP: Digital signal processor, arithmetic unit, its main application is real-time, quickly realize various digital signal processing algorithms.

The design of the DC leakage sensor mainly includes the design of the Soc chip, the design of the magnetic core and the winding, and the design of the circuit, and the device reliability design of the DC leakage sensor is carried out. Figure 13 shows a DC leakage sensor manufactured with the chips in Figures 10 and 11.

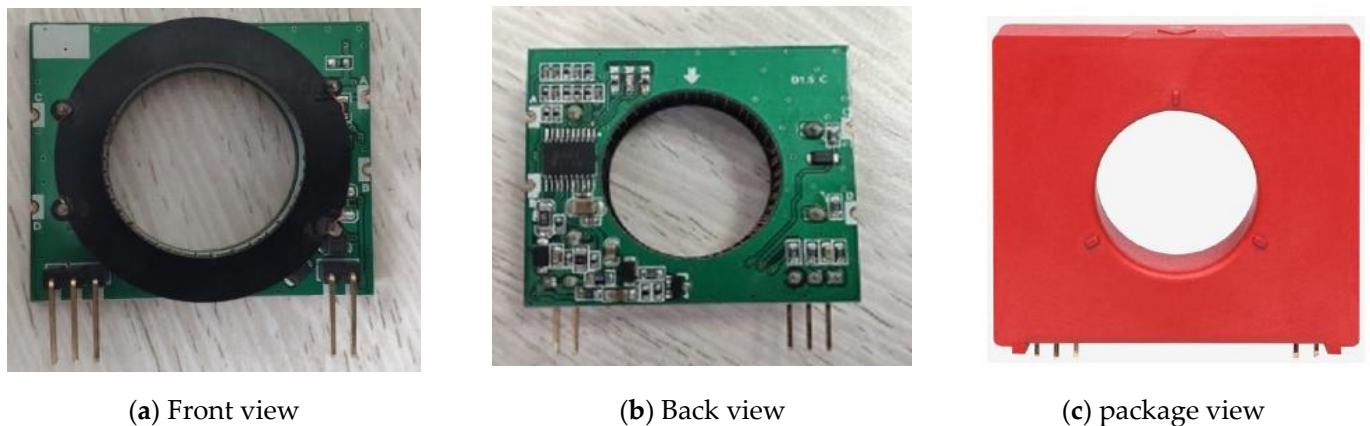


**Figure 13.** Dc leakage sensor real figure.

## 5. DC Leakage Protection Circuit Breaker Simulation and Experiment

Figure 14 shows the prototype of DCCB. Figure 15 shows the cloud diagram of magnetic density distribution of DCCB at different times.

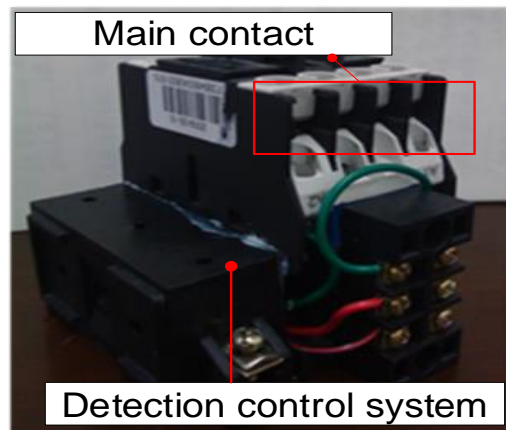


Figure 14. DC leakage circuit breaker prototype.

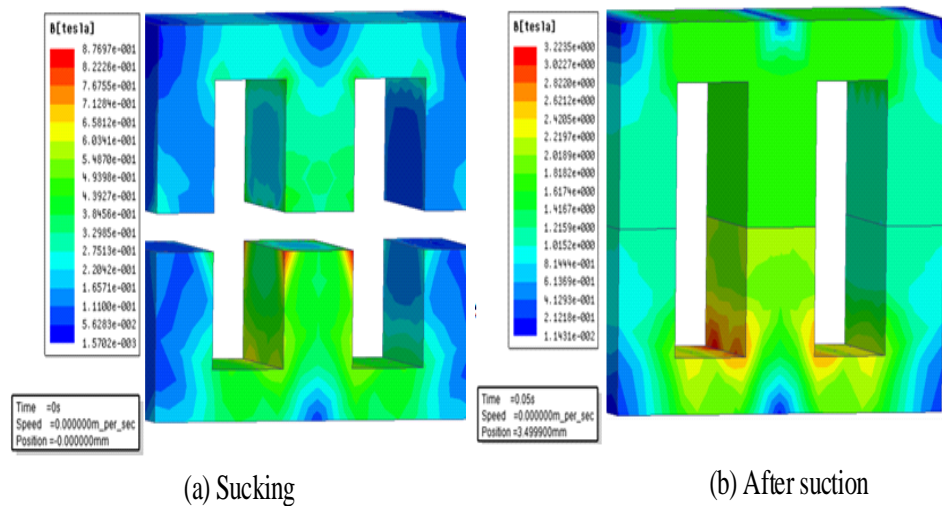


Figure 15. Contactor magnetic density distribution cloud at different times.

As can be seen from Figure 16, when the displacement of the moving iron core is 3.5 mm, the action time is 50 ms. At this time, if the excitation current is increased, the action time of the moving iron core will be shorter, which is in line with the action law of the DC leakage protector.

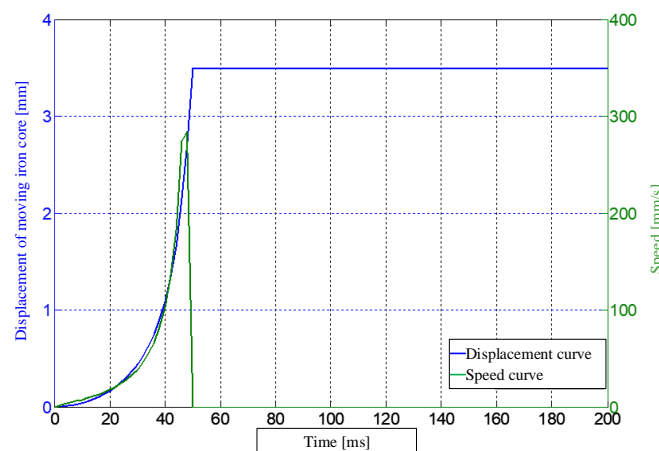


Figure 16. Mobile dynamic core displacement and velocity curve.

Figure 16 shows the moving displacement and speed curve of the moving core, and Figure 17 shows the change curve of the moving core and spring reaction force with time.

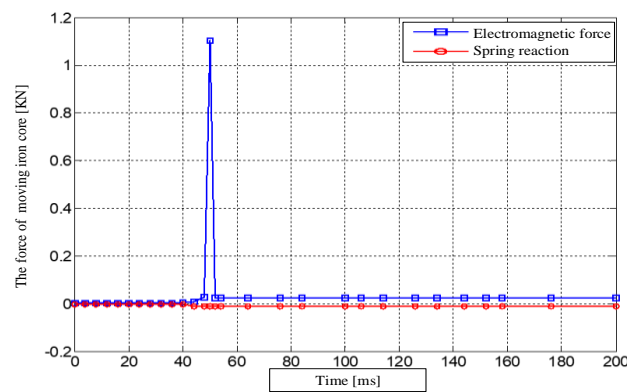


Figure 17. Dynamic core and spring force changing with time curve.

The test steps in the results of Figures 16 and 17 are as follows:

First, let samples 1–5 represent 5 samples of DC leakage protectors manufactured, respectively, then pass a high-precision current to the current sensor through the Agilent 34970A power supply, and measure the output voltage of the current sensor with a high-precision multimeter, as shown in Figure 18. As can be seen from Figure 18, the current sensor accuracy is within 1%, and can effectively detect the leakage current of 30 mA–600 mA.

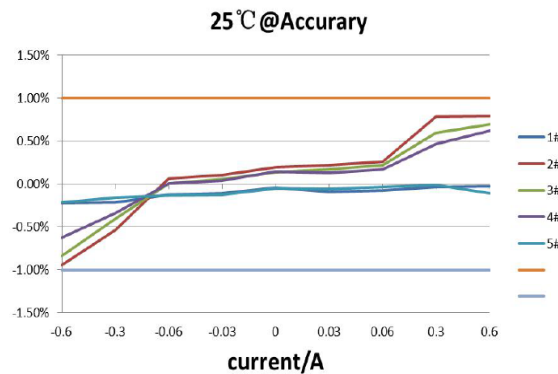


Figure 18. The diagram of accuracy curve.

Secondly, the frequency response test was carried out. Single magnetic ring single winding was adopted, and 3.7 kHz frequency excitation was used. After the measuring module is switched on for 10 min at rated voltage. Through the signal generator, the signal amplifier, the current valid value of the IPN is passed into the sensor input terminal, then scans the frequency segment of 0 Hz–2 kHz. Figure 19 shows the frequency response diagram.

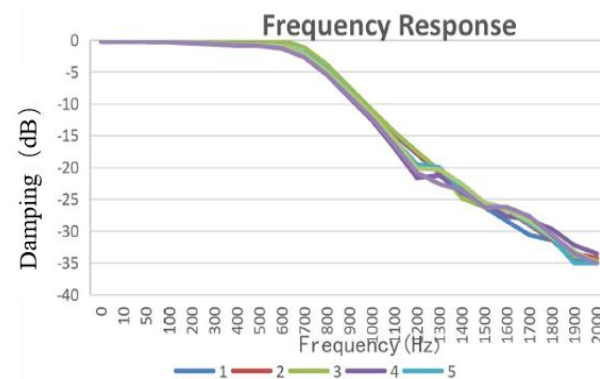


Figure 19. The diagram of frequency response.

As shown in Figure 19, after testing and verification, the frequency response of the DC leakage sensing monitoring module proposed in this paper is 700 Hz (−3 dB).

Finally, test the response time. Under the condition of rated voltage, the DC leakage sensing monitoring module connects the power to the sensor for 10 min, and then passes the signal generator and signal amplifier to the current with a frequency of 50 Hz and a current of  $I_{PN}$  input the sensor input terminal, use RIGOL-MSO5354 oscilloscope (oscilloscope parameters: bandwidth 35 M, 5 Gsa/s) to measure the time required for the sensor to reach 10% and 90% of the final value. Figure 20 shows the test device for this experiment.

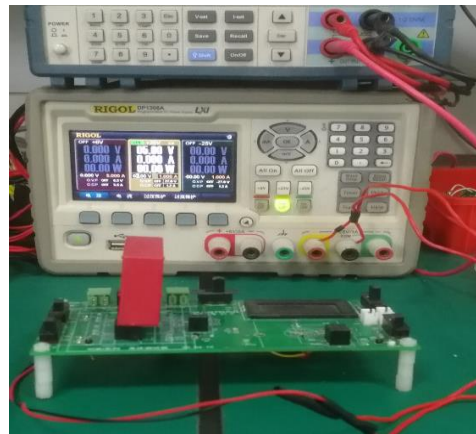


Figure 20. The diagram of testing device.

As shown in Figure 21, the pink line represents a given signal, and the yellow line represents the actual output signal. We can get that the response time of DC leakage sensor is 520  $\mu$ s when it reaches 10% and 990  $\mu$ s when it reaches 90%, which meets the system requirements.



(a) (10%)



(b) (90%)

Figure 21. DC leakage time response of the sensor.

The output of the DC leakage sensor is a voltage analog signal. The leakage current of the test system mainly generates a  $\pm 0.03$  A,  $\pm 0.3$  A,  $\pm 0.6$  A current signal through the power supply to simulate the leakage signal. Figure 20 shows the schematic diagram of leakage current detection system.

As shown in Figure 22, The current  $I_1$  changes, causing the voltage  $V_H$  to change, Voltage signal is extracted and amplified by differential amplifier and then enhanced by proportional amplifier, and then output the  $V_{out}$ .

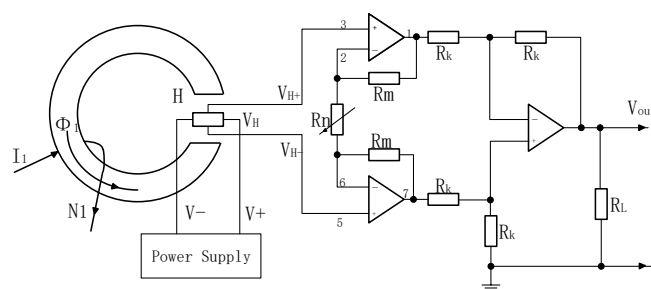


**Figure 22.** The schematic diagram of Leakage current detection.

Table 1 shows the comparison of the measurement results of the DC leakage sensor. Among them, sample 1–sample 5 represents the five DC leakage protector samples manufactured. Through the 34970A power supply of Agilent company, the current sensor is fed with high-precision current, the input current is changed, and the output voltage of the current sensor is measured. The following data are obtained through the test.

**Table 1.** DC leakage sensor measurement results.

Temperature Range/°C	Current Range/A	Voltage Range/A	Measured Current/A	Sample 1 /V	Sample 2 /V	Sample 3 /V	Sample 4 /V	Sample 5 /V
25	0.03	2.6	0.03004	2.5964	2.6087	2.6069	2.6051	2.5977
25	0.06	2.7	0.0599	2.6969	2.7105	2.7088	2.7067	2.6985
25	0.3	3.5	0.29972	3.4987	3.5313	3.5238	3.5185	3.4994
25	0.6	4.5	0.59967	4.4989	4.5317	4.5278	4.5247	4.4994
25	0	2.5	0	2.4982	2.5079	2.5054	2.5058	2.4979
25	−0.03	2.4	−0.03003	2.3955	2.404	2.4023	2.4015	2.3951
25	−0.03	2.3	−0.0599	2.2949	2.3024	2.3003	2.3001	2.2947
25	−0.3	1.5	−0.29974	1.4915	1.4786	1.4837	1.4865	1.4935
25	−0.6	0.5	−0.59969	0.4909	0.4623	0.4665	0.475	0.4913

As shown in Table 1, the output signal of DC leakage sensor is leakage current. According to the leakage signal, the action of two-phase magnetic materials can be guided. When the leakage current reaches the protection action value, the nano two-phase magnetic materials demagnetize to change the contact from closed state to open state to complete the protection action.

It can be seen from Table 1 that the accuracy of the module at room temperature is within 1%, which meets the system requirements. Additionally, it can effectively detect the leakage current in the range of 30 mA–600 mA. The correctness of the proposed scheme is verified.

## 6. Conclusions

This paper develops a smart/energy-saving DC leakage protection circuit breaker based on nano-two-phase magnetic material and detection control technology, which gives the preparation, processing method and characteristic parameters of nano-two-phase magnetic materials; secondly, DC leakage detection technology is launched. Research, a design process of a magnetic ring, a winding, etc. Finally, a smart/energy-saving DCCB is manufactured with the related experiments, which is obtained:

- (1) When the nano two-phase magnetic material is characterized by permanent magnetic characteristics, the magnetic induction intensity of the operating mechanism of intelligent/energy-saving DCCB leakage protection circuit breaker is 1.5 T, reaching a stable pull-in state.
- (2) When the DC leakage sensor reaches 10%, the response time is 520  $\mu$ s and when it reaches 90%, the response time is 990  $\mu$ s. Therefore, it can be judged that the equipment can make the leakage outlet mechanism act quickly to achieve the purpose of leakage protection.

- (3) The smooth implementation of this paper provides a new idea about the product development of energy-saving DCCB.

**Author Contributions:** Writing—original draft, L.H.; Writing—review & editing, D.C., T.L., M.Z. and H.R. All authors have read and agreed to the published version of the manuscript.

**Funding:** This research was funded by Department of Education of Liaoning Province, grant number [LGD2016011] and State Grid Corporation of China (China), grant number [kj2019-013-II].

**Conflicts of Interest:** The authors declare no conflict of interest.

## References

1. Xiao, J.; Wang, P.; Setyawan, L. Hierarchical Control of Hybrid Energy Storage System in DC Microgrids. *IEEE Trans. Ind. Electron.* **2015**, *62*, 4915–4924. [[CrossRef](#)]
2. Haibo, L.; Yuming, Z.; Guowei, L.; Shiyong, J.; Zhengjia, Z. Energy efficiency comparison of AC and DC distribution systems in commercial buildings based on time series simulation. *J. Electrotech.* **2020**, *35*, 4194–4206.
3. Liao, J.; Zhou, N.; Wang, Q.; Li, C.; Yang, J. Definition and correlation analysis of power quality indicators of DC distribution network. *Chin. J. Electr. Eng.* **2018**, *38*, 6847–6860+7119.
4. Jung, J.H.; Kim, H.S.; Ryu, M.H.; Baek, J.W. Design methodology of bidirectional CLLC resonant converter for high-frequency isolation of DC distribution systems. *IEEE Trans. Power Electron.* **2013**, *28*, 1741–1755. [[CrossRef](#)]
5. Gollee, R.; Gerlach, D. An FEM-Based Method for Analysis of the Dynamic Behavior of AC Contactors. *IEEE Trans. Magn.* **2000**, *36*, 1337–1340.
6. Minfu, L.; Jinqiang, H.; Guowei, G.; Shanjun, W.; Xiongying, D. Development and research status of hybrid circuit breaker at home and abroad. *High Volt. Eng.* **2016**, *42*, 1688–1694.
7. Shimin, X.; Chaochao, C.; Yi, J.; Jian, S.; Tao, W.; Jiali, H.; Ying, W. A Summary of Research on DC Distribution System Protection Technology. *Proc. Chin. Soc. Electr. Eng.* **2017**, *37*, 966–978.
8. Luhui, L.; Zhihao, Y.; Lijun, F.; Youxing, X.; Nan, W. Research & Development Status and Prospects of Fast DC Circuit Breakers. *Proc. Chin. Soc. Electr. Eng.* **2017**, *37*, 966–978.
9. Junjia, H.; Zhao, Y.; Wenting, Z.; Shai, F.; Xinlin, Y.; Huan, P. Summary of technology development of DC Breaker Technology. *South Power Syst. Technol.* **2015**, *9*, 9–15.
10. Xiaoguang, W.; Bingjian, Y.; Guangfu, T. Technology Development and Engineering Practice of High Pressure DC Breaker Technology. *Power Syst. Technol.* **2017**, *41*, 1319–1323.
11. Shede, P.; Mane, S. Leakage current sensing techniques. In Proceedings of the 2017 Third International Conference on Sensing, Signal Processing and Security (ICSSS), Chennai, India, 4–5 May 2017; pp. 181–185. [[CrossRef](#)]
12. Kudo, T.; Kuribara, S.; Takahashi, Y. Wide-range ac/dc earth leakage current sensor using fluxgate with self-excitation system. In Proceedings of the SENSORS, 2011 IEEE, Limerick, Ireland, 28–31 October 2011; pp. 512–515. [[CrossRef](#)]
13. Schade, E.; Shmelev, D.L. Numerical Simulation of High-Current Vacuum Arcs with an External Axial Magnetic Field. *IEEE Trans. Plasma Sci.* **2003**, *31*, 890–901. [[CrossRef](#)]
14. Zheng, S.; Kheirollahi, R.; Pan, J.; Xue, L.; Wang, J.; Lu, F. DC Circuit Breakers: A Technology Development Status Survey. *IEEE Trans. Smart Grid.* **2021**. [[CrossRef](#)]
15. Watanabe, H.; Itoh, J.-I.; Koike, N.; Nagai, S. PV Micro-Inverter Topology Using LLC Resonant Converter. *Energies* **2019**, *12*, 3106. [[CrossRef](#)]
16. Rezaei-Zare, A.; Iravani, R.; Sanaye-Pasand, M.; Mohseni, H.; Farhangi, S. An Accurate Current Transformer Model Based on Preisach Theory for the Analysis of Electromagnetic Transients. *IEEE Trans. Power Deliv.* **2008**, *23*, 233–242. [[CrossRef](#)]
17. Nana, D.; Weijie, X.; Yongjian, L.; Shuhong, W.; Jianguo, Z. Simulation of Magnetic Properties of Soft Magnetic Composites Based on Limiting Hysteresis Loop Method. *J. Electrotech. Technol.* **2018**, *33*, 4739–4745. [[CrossRef](#)]
18. Andreev, M.; Askarov, A.; Suvorov, A. Design of the magnetic hysteresis mathematical model based on Preisach theory. *Electr. Eng.* **2019**, *101*, 3–9. [[CrossRef](#)]
19. Changxi, Y.; Qiong, X.; Xue, L.; Huan, W.; Kai, Z.; Hao, L. Zero-flux AC and DC current sensor based on fluxgate principle. *Electr. Meas. Instrum.* **2017**, *54*, 73–77.